Power System Technology
ISSN:1000-3673

Received: 16-04-2025 Revised: 05-05-2025 Accepted: 22-07-2025

# Numerical Investigation of Non-Newtonian Hybrid Nano fluid Wall Jet Flow with Heat and Mass Transfer over a Permeable Stretching Surface

**A.Shareef[1] , Madan Mohan Reddy[2],K.Rajarajeswari[3], C.P.Sekhar [4], N Rajassekhar Reddy[5]**

[1,3,4] Assistant Professor ,Dept.of Mathematics Ashoka Women's Engineering College,Kurnool,l -518002, Andhra Pradesh, India
[2]Assistant Professor ,Dept.of Mathematics Dr.K.V.Subbareddy Engineering college,Kurnool,l -518002, Andhra Pradesh, India
[5]Assistant Professor,Dept.of Mathematics Santhiram Engineering Eollege Nandyal ,Andharapradesh,India

***Abstract***:-

Wall jet flows play a vital role in thermal regulation of electronic components, where a high-speed fluid stream is directed from a narrow slit along a flat surface to enhance heat dissipation. This method effectively boosts heat transfer rates, making it highly suitable for managing thermal loads in compact electronic systems. The present study introduces a new numerical approach to examine non-Newtonian wall jet flow of a hybrid Nano fluid, characterized by the suspension of silver (Ag) and copper (Cu) nanoparticles within a sodium alginate base fluid. A key contribution of this work lies in its comparative analysis of such a hybrid Nano fluid flow over a permeable, stretching surface, incorporating the influences of Brownian motion and thermophoresis effects. The analysis considers two different flow regimes: suction ($S > 0$) and injection ($S < 0$). Through appropriate similarity transformations, the governing partial differential equations are converted into a system of ordinary differential equations. These are then solved numerically using the bvp4c solver in MATLAB. Graphical illustrations are employed to explore the effects of various dimensionless parameters on the velocity, temperature, and concentration distributions. The results indicate that increasing the porosity parameter leads to a decrease in skin friction, thereby reducing interlayer resistance and facilitating smoother fluid flow—particularly prominent in the suction case. Moreover, an increase in the thermophoresis parameter causes a decline in the Nusselt number due to the formation of a thicker thermal boundary layer, which impedes convective heat transfer; this effect is more pronounced in the injection scenario as fresh fluid thickens the layer. Conversely, the Sherwood number rises with higher thermophoresis values, as the injection process promotes better dispersion and mixing of nanoparticles, thereby improving mass transfer efficiency. These findings offer valuable insights for the design of advanced cooling strategies in microelectronic devices, turbine blade cooling, and other thermal management applications.

Power System Technology
ISSN:1000-3673
Received: 16-04-2025 Revised: 05-05-2025 Accepted: 22-07-2025

***Keywords:***Wall jet flow, Hybrid Nano fluid, Non-Newtonian fluid, Brownian motion, Thermophoresis, Permeable stretching surface,

## 1. Introduction

Hybrid nanofluids are widely recognized for their enhanced thermal performance, making them advantageous for applications in transformer cooling, thermal energy systems, and automotive technologies. Their superior heat transfer capabilities contribute to increased energy efficiency, reduced operational costs, and improved system performance. Owing to these benefits, hybrid nanofluids have garnered significant interest among researchers. Several studies have addressed heat and mass transfer behavior in various boundary layer flows involving hybrid nanoparticles (Ganga et al. 2023; Uddin et al. 2021; Kumar et al. 2018a; Upreti et al. 2024). For instance, Ganga et al. (2025) examined the influence of magnetohydrodynamics (MHD) and nonlinear radiation in a Maxwell hybrid nanofluid flow past an exponentially expanding sheet, concluding that hybrid nanofluids achieve better heat transfer rates compared to standard nanofluids. Similarly, Kumar et al. (2023a) investigated the effect of nanoparticle shape in hybrid nanofluids flowing over a wedge and observed that blade- and brick-shaped nanoparticles offered more efficient heat transfer than spherical ones. Aly et al. (2022) analyzed the role of mass transpiration and radiation in hybrid nanofluid wall jet flows over stretched surfaces and found that increasing the nanoparticle volume fraction improves the velocity profile under suction. Yaseen et al. (2023) applied an Eyring-Powell hybrid nanofluid model to solve MHD wall jet flow over a stretching surface, reporting that the presence of a magnetic field significantly reduces the skin friction coefficient.

Casson fluids, known for their viscoelastic properties, demonstrate improved thermal transport. Research by Varatharaj et al. (2024) and Mahabaleshwar et al. (2024a) revealed that thermal radiation and magnetic effects considerably influence convective heat and mass transfer in Casson fluids. Shamshuddin et al. (2023) studied the inclusion of Ohmic heating and mixed convection in hybrid nanofluid flow over an exponentially stretching surface and reported an increase in velocity for both mono and hybrid nanofluids with rising mixed convection. Mahabaleshwar et al. (2024b) examined the impact of inclined MHD and heat sources/sinks on Casson hybrid nanofluid flow through permeable stretching/shrinking surfaces. Alzahrani et al. (2022) focused on Glauert-type wall jets of radioactive Cassonnanofluids under suction and slip boundary conditions and found that an increase in the Casson parameter lowered the heat transfer rate, while enhanced radiation had the opposite effect.

In nanotechnology, Thermophoresis and Brownian motion are critical mechanisms for manipulating heat and mass transport, especially in complex fluids such as polymeric solutions and biological fluids. These effects substantially alter flow behavior. Babu et al.

Power System Technology
ISSN:1000-3673
Received: 16-04-2025 Revised: 05-05-2025 Accepted: 22-07-2025

(2024) investigated their combined influence on a Williamson nanofluid under MHD and chemical reaction conditions, finding increased thermal distribution with stronger Brownian and thermophoretic effects. Similarly, Ibrahim et al. (2023) examined Hiemenz flow under radiative, MHD, and chemical reaction influences and reported significant thermal variations due to these phenomena. Lone et al. (2023) explored Thermophoresis and Brownian motion in a bioconvective MHD flow of Casson hybrid nanofluid across an exponentially stretching surface with porous media, while Sudarmozhi et al. (2024) analyzed Maxwell fluid flow over a stretching sheet with melting heat and chemical reaction. They found that higher Brownian motion reduced concentration, whereas increased Thermophoresis had the opposite effect.

Suction and injection mechanisms are essential in modifying flow fields, optimizing thermal performance, and adjusting boundary layers. Numerous investigations have highlighted their importance in various fluid flow configurations (Kumar et al. 2020a; Ram Sharma and Jain 2024; Mahmood et al. 2024). Köten et al. (2024) examined ternary nanofluid flow across stretching/shrinking sheets and found that temperature variation under injection is more pronounced compared to suction. Mahabaleshwar et al. (2024c) compared numerical and neural network-based models to assess suction/injection effects under MHD, chemical reaction, and heat source scenarios, revealing higher heat transfer during blowing and reduced mass transfer under injection.

Wall jet flows are encountered when a fluid is released from an opening along a surface, creating radial layers composed of inner and outer flow regions. These flows are crucial in various engineering applications for their ability to control heat and mass transport. Mahros et al. (2023) investigated wall jet flow of hybrid nanofluids across a stretched surface influenced by MHD and showed that suction can cause a velocity reduction by diverting fluid into void regions. Aly et al. (2024) studied laminar wall jet convective flows and observed how suction and injection influence flow characteristics. Khan et al. (2023a) modeled an Eyring-Powell nanofluid wall jet flow on a vertically stretchable sheet with variable heat sources. Khan et al. (2023b) employed the Brinkman-extended Darcy model to assess the impact of radiation and activation energy in wall jet flows with nano-lubricants, highlighting that the permeability and porosity parameters initially influence and eventually enhance velocity.

The bvp4c method provides a reliable tool for solving complex boundary value problems in fluid dynamics. Its effectiveness lies in its precision, simplicity in MATLAB, and capacity to handle nonlinear systems relevant to heat and mass transfer modeling. Chaurasiya et al. (2024) applied the bvp4c technique to study the effects of magnetic fields in Marangoni convection over a rotating disk using self-rewetting fluids. Kumar and Ray (2022) examined nanoparticle shape and Hall effects in MHD hybrid nanofluid flow over a rotating disk under entropy generation, also using bvp4c. Nasir et al. (2024) used this method to analyze ternary nanofluid flow over a stretching Riga plate in the presence of a heat source/sink and viscous dissipation. In another study, Kumar et al. (2023b) applied bvp4c to solve the unsteady flow

Power System Technology
ISSN:1000-3673
Received: 16-04-2025 Revised: 05-05-2025 Accepted: 22-07-2025

of hybrid nanofluid over a rotating sphere under mixed convection with heat absorption/generation.

Despite extensive literature on hybrid nanofluid wall jet flows, no prior work has comprehensively addressed the comparative effects of suction and injection in a porous medium considering Brownian motion and Thermophoresis. Given the relevance of wall jets in electronic cooling, jet impingement, vehicle thermal systems, and high-temperature fluid processes, this gap is notable. Therefore, the present study explores the influence of suction and injection on a wall jet hybrid nanofluid flow over a stretching surface within a porous medium, accounting for Thermophoresis and Brownian motion. The model is governed by partial differential equations, reduced to ordinary differential equations via Glauert transformations, and solved numerically using the bvp4c method (al. 2017; Khan Usafzai et al. 2023; Jafarimoghaddam and Shafizadeh 2019; Uddin et al. 2024; Kumar et al. 2020b).

## 2.Mathematical Formulation:

A schematic diagram of the considered physical configuration is depicted in Fig. 1, representing a two-dimensional, steady, incompressible laminar wall jet flow of a sodium alginate-based hybrid nanofluid containing Ag and Cu nanoparticles. The flow occurs over a stretched surface subjected to the influence of a porous medium, Brownian motion, and thermophoresis. The effects on velocity, temperature, and nanoparticle concentration are examined under both suction (S>0) and injection (S<0) scenarios.

Let u and v be the velocity components in the xxx- and y-directions, respectively. The fluid temperature TTT is maintained at a constant wall temperature Tw, while T∞ denotes the ambient temperature. Similarly, Cw andC∞ represent the nanoparticle concentrations at the wall and at infinity, respectively.

The Casson fluid model is utilized to characterize the rheological behavior of the non-Newtonian fluid. The constitutive relation for the Casson fluid is expressed as follows:

$$\tau = \left(\mu_b + \frac{p_y}{\sqrt{\pi^2}}\right) e_{ij} 2, \pi_c < \pi; \tau = \left(\mu_b + \frac{p_y}{\sqrt{2\pi_c}}\right) 2e_{ij},$$

$\pi_c > \pi$. Where, $\pi$ - represents the product of the deformation rate component and $(\pi_c, \mu_b)$ is a significant assessment of $\pi$and plastic dynamic viscosity of a non-Newtonian model, $e_{ij}$ is the $(i,j)^{th}$ component of the deformation rate, $p_y$ represents yield stress of fluid. The following governing equations are possibly formed using the aforementioned assumptions see (Ali Zaidi et al. 2017; Khan Usafzai et al. 2023; Jafarimoghaddam and Shafizadeh 2019; Uddin et al. 2024; Kumar et al. 2020b).

$$\frac{\partial v}{\partial y} + \frac{\partial u}{\partial x} = 0, \quad (1)$$

Power System Technology
ISSN:1000-3673
Received: 16-04-2025 Revised: 05-05-2025 Accepted: 22-07-2025

$$v\frac{\partial u}{\partial y}+u\frac{\partial u}{\partial x}=v_{hnf}\left(1+\frac{1}{\beta}\right)\frac{\partial^2 u}{\partial y^2}-\frac{v_{hnf}u}{K(x)}, \quad (2)$$

$$v\frac{\partial T}{\partial y}+u\frac{\partial T}{\partial x}=\frac{\partial^2 T}{\partial y^2}\left(\frac{k_{hnf}}{(\rho Cp)_{hnf}}\right)$$

and following are the corresponding boundary conditions

$$\text{at } y=0 u=u_w, v=v_w, T=T_w, C=C_w, \quad (5)$$

At$y\to\infty: u\to u_\infty, T\to T_\infty, C\to C_\infty$.

Here, ( $\mu, v$ ) represents dynamic and kinematic viscosity, $\beta$ denotes Casson parameter, $\rho$ Represents fluid's density, $k$ is the thermal conductivity, $Cp$ means specific heat capacity, $K(x)=\hat{k}_o x^{3/2}$ denote variable permeable constraint, $\bar{\tau}$ signifies heat capacity ratio, $(D_b, D_T)$ is the coefficient of Brownian diffusion and thermophoretic diffusion,

Table 1:Thermophysical features of base fluid and hybrid nanoparticle (Kumar et al. 2018b, 2023c; Maboodet al. 2020)

| Physical properties | Sodium Alginate | $Ag$ | $Cu$ |
|---|---|---|---|
| $\rho(\text{kgm}^{-3})$ | 989 | 10,500 | 8933 |
| $Cp(\text{Jkg}^{-1}\text{K}^{-1})$ | 4175 | 235 | 385 |
| $k(\text{kgms}^{-3}\text{K}^{-1})$ | 0.6376 | 429 | 401 |

Table 2: Thermal characteristics of hybrid nanoparticles

| | |
|---|---|
| ( $\mu$ ) | $\frac{\mu_{\text{hnf}}}{\mu_f}=\frac{1}{(1-\phi_1)^{2.5}(1-\phi_2)^{2.5}},$ |
| Dynamic viscosity | |
| ( $\rho$ ) | $\frac{\rho_{hnf}}{\rho_f}=\left[\left(\phi_1\frac{\rho_1}{\rho_f}+(1-\phi_1)\right)(1-\phi_2)+\phi_2\frac{\rho_2}{\rho_f}\right],$ |
| Density | |
| ( $\rho C$ p) | $\frac{(\rho Cp)_{\text{hnf}}}{(\rho Cp)_f}=$ |

Power System Technology
ISSN:1000-3673
Received: 16-04-2025 Revised: 05-05-2025 Accepted: 22-07-2025

| | |
|---|---|
| Heat capacity | $\left[\left(\phi_1 \frac{(\rho Cp)_1}{(\rho CP)_f} + (1-\phi_1)\right)(1-\phi_2) + \phi_2 \frac{(\rho Cp)_2}{(\rho CP)_f}\right]$, |
| (k) | $\frac{k_{nnf}}{k_{nf}} = \frac{k_2 + k_f - \phi_2(k_f - k_2)}{k_2 + k_f + \phi_2(k_f - k_2)}$, |
| Thermal conductivity | $\frac{k_{nf}}{k_f} = \frac{k_1 + k_f - \phi_1(k_f - k_1)}{k_1 + k_f + \phi_1(k_f - k_1)}$ |

$v_w = -v_f^{1/2} x^{-3/4} S$. Table 2 provides the thermophysical characteristics of conventional fluid (Sodium alginate) and hybrid nanoparticles ( and$Cu$ ) and the data on the hybrid nanoparticles thermophysical characteristics is given in Table 3.

Here, the similarities followed by ref Khan et al. 2023b were used to facilitate scrutinizing the current wall jet model.

$\eta = \frac{y}{\sqrt{v_f}} x^{-3/4}, u = \frac{4}{\sqrt{x}} F', v = -\sqrt{v_f} x^{-3/4}(F - 3\eta F'),$

$G(T_w - T_\infty) = T - T_\infty, H(C_w - C_\infty) = C - C_\infty.$

Using Eqs. (7) and (8) with thermophysical properties in Table 2, Eqs. (2)-(4) are transformed as

$\frac{1}{A_1 A_2}\left(1 + \frac{1}{\beta}\right) F''' + 2F'^2 + FF'' - \frac{1}{A_1 A_2} \alpha F' = 0,$

$\frac{k_{hnf}}{k_f} \frac{1}{\mathrm{Pr} A_3} G'' + FG' + NbH'G' + NtG^2 = 0,$

$H'' + Le\mathrm{Pr}FH' + \frac{Nt}{Nb} G'' = 0.$

and

$F'(0) = 1, F(0) = S, G(0) = 1, H(0) = 1,$

$F'(\infty) = 0, G(\infty) \to 0, H(\infty) \to 0.$

where, $\alpha$ is the porosity parameter, $\mathrm{Pr} = \frac{v_f}{\alpha_f}$ indicates Prandtl number, $Nb = \frac{D_b \tau \Delta C}{v_f}$ and $Nt = \frac{D_T \tau \Delta T}{T_\infty v_f}$ indicates Brownian motion and Thermophoresis parameters respectively, $Le = \frac{\alpha_f}{D_b}$ is Lewis number and $S$ represents injection/suction parameter.

The engineering quantities with their reduced form obtained in this study are as follows:

$$Cf = \frac{1}{\rho_f u_w^2}\left(1 + \frac{1}{\beta}\right) \mu_{hnf} \left.\frac{\partial u}{\partial y}\right|_{y=0}$$

where, $\mathrm{Re}_x = \frac{x u_w}{v_f}$ is the local Reynolds number.

Power System Technology
ISSN:1000-3673
Received: 16-04-2025 Revised: 05-05-2025 Accepted: 22-07-2025

**3.Methodology:**

This section outlines the methodology employed to obtain numerical solutions and verify the accuracy of the implemented code. The bvp4c function in MATLAB is utilized for solving boundary value problems (BVPs) related to ordinary differential equations (ODEs). This method offers a robust and accurate approximation of the solution while ensuring that boundary conditions are satisfied at both ends of the domain. A schematic representation of the methodological workflow is illustrated in Fig. 2.
The computational procedure involves the following steps:

**a. Transformation of Equations**: The governing partial differential equations (PDEs) are initially transformed into ordinary differential equations (ODEs) using similarity variables.

**b. Conversion to First-Order System**: The resulting higher-order ODEs are then reformulated into a system of first-order equations by introducing auxiliary variables. This step is necessary to facilitate numerical integration using the bvp4c solver.

$\langle F = \Theta_1, F' = \Theta_2, F'' = \Theta_3, G = \Theta_4, G' = \Theta_5, H = \Theta_6, H' = \Theta_7 \rangle$,
c. Write MATLAB syntax: Formulate the MATLAB syntax for the reduced Eqs. (9) to. (11) and boundary conditions (12) and (13) to prepare for simulation.

For reduced equations and BCs, the MATLAB syntax is employed as shown below.
$\Theta_3' = -\frac{A_1 A_2}{\left(1+\frac{1}{\beta}\right)}\left(2\Theta_2^2 + \Theta_1\Theta_3 - \frac{1}{A_1 A_2}\alpha\Theta_2\right)$,
$\Theta_5' = -\frac{\mathrm{Pr} k_f A_3}{k_{hnf}}(\Theta_1\Theta_5 + Nb\Theta_7\Theta_5 + Nt\Theta_5^2)$,
$\Theta_7' = -\left(\mathrm{LePr}\Theta_1\Theta_7 + \frac{Nt}{Nb}\Theta_5 \quad '\right)$.
and
$\Theta_2(0) = 1, \Theta_1(0) = S, \Theta_4(0) = 1, \Theta_6(0) = 1$,
$\Theta_2(\infty) = 0, \Theta_4(\infty) \to 0, \Theta_6(\infty) \to 0$.
d. Insertion of reduced equations and boundary conditions: Input the relevant reduced Eqs. (9) to (11) into the bvp-4c solver to obtain the numerical solutions, specifying the syntax as "solution = bvp-4c (@BVP, @BC, solutioninit)", where "@BVP and @BC" define the equations and boundary conditions respectively. The preliminary mesh points and the primary solution approximation at these locations are coded using the "solutioninit" function.

Power System Technology
ISSN:1000-3673
Received: 16-04-2025 Revised: 05-05-2025 Accepted: 22-07-2025

Table 3: Comparison of present work with Khanet al. (2023b) and Waini et al. (2021) work in the absence of $\alpha, S$ with $\beta \to \infty, A_1 = A_2 = 1$

| $\phi$ | Waini et al. (2021) | Khan et al. (2023b) | Present study outcomes |
|---|---|---|---|
| 0.0 | 0.2222 | 0.2222 | 0.2222 |
| 0.035 | - | 0.3178 | 0.3180 |
| 0.037 | - | 0.3656 | 0.3659 |
| 0.039 | - | 0.4132 | 0.4138 |

e. Execute solver: After substituting the parametric values $= 1.0, S = \pm 0.5, \alpha = 1.5, \mathrm{Pr} = 6, 0.01 \leq \phi_1 = \phi_2 \leq 0.03, Le = 0.8, Nt = 0.3, Nb = 0.3$, and setting mesh size at 100 , execute the solver to compute the solution.

This section presents the physical interpretation of various dimensionless parameters involved in the current boundary value problem. The study investigates hybrid nanofluid wall jet flow over a stretching surface by analyzing the effects of key parameters: porosity parameter ($1.5 \leq \alpha \leq 2.5$), Casson parameter ($0.5 \leq \beta \leq 0.9$), Thermophoresis parameter ($0.1 \leq \mathrm{Nt} \leq 0.2$), and Brownian motion parameter ($0.5 \leq \mathrm{Nb} \leq 0.9$). The suction/injection parameter is fixed at $\mathrm{S} = \pm 0.5$ to examine both suction ($\mathrm{S} > 0$) and injection ($\mathrm{S} < 0$) scenarios. The governing nonlinear partial differential equations are transformed into ordinary differential equations using similarity transformations and solved numerically using MATLAB's bvp4c function.

Figures 1 through 9 illustrate the influence of these parameters on the velocity F′(η)F'(\eta)F′(η), temperature G′(η)G'(\eta)G′(η), and concentration H′(η)H'(\eta)H′(η) profiles, along with engineering quantities such as the skin friction coefficient (Cf), Nusselt number (Nu), and Sherwood number (Sh).

Figure 1: illustrates the effect of the porosity parameter α on the velocity profile F′(η)F'(\eta)F′(η). As α increases, the velocity decreases. This is because higher porosity values suggest a more permeable medium, offering multiple flow pathways that disrupt and dissipate the momentum of the fluid, thereby reducing the overall flow velocity.

Power System Technology
ISSN:1000-3673
Received: 16-04-2025 Revised: 05-05-2025 Accepted: 22-07-2025

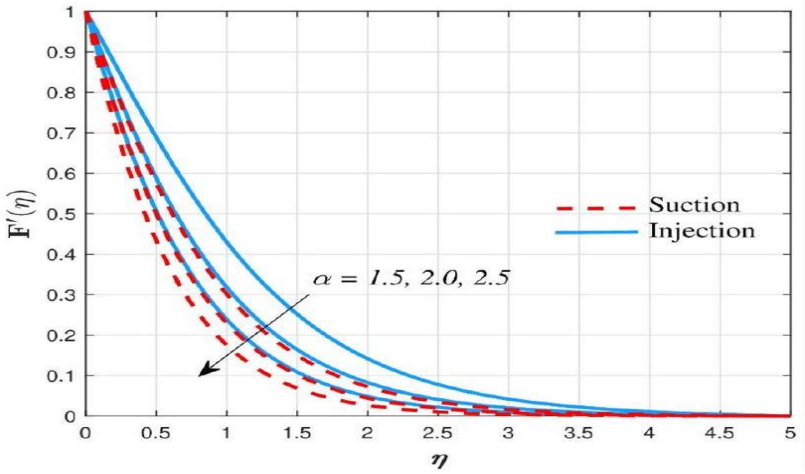


Fig. 1 Effect of $\alpha$ over $F'(\eta)$ profile

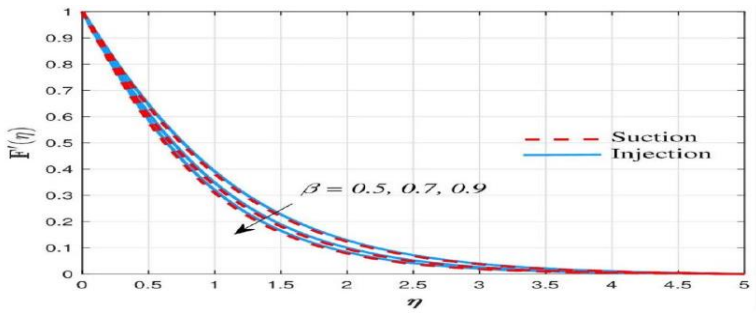


Fig. 2 Effect of $\beta$ over $F'(\eta)$ profile

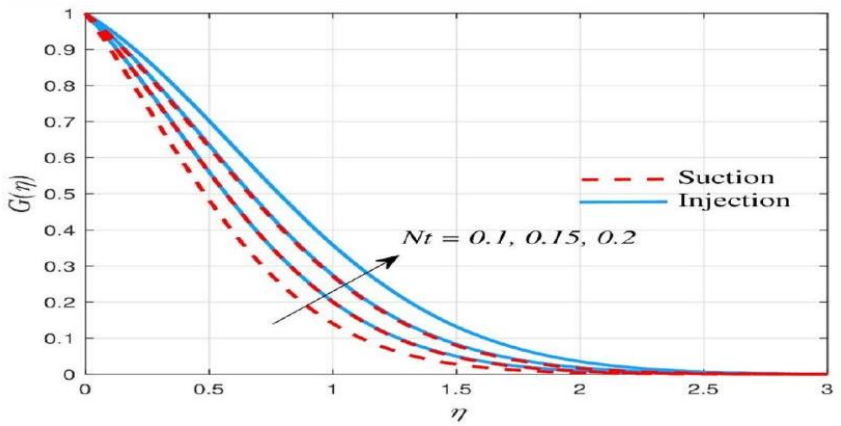


Fig. 3 Impact of $Nt$ over $G'(\eta)$ profile

Power System Technology
ISSN:1000-3673
Received: 16-04-2025 Revised: 05-05-2025 Accepted: 22-07-2025

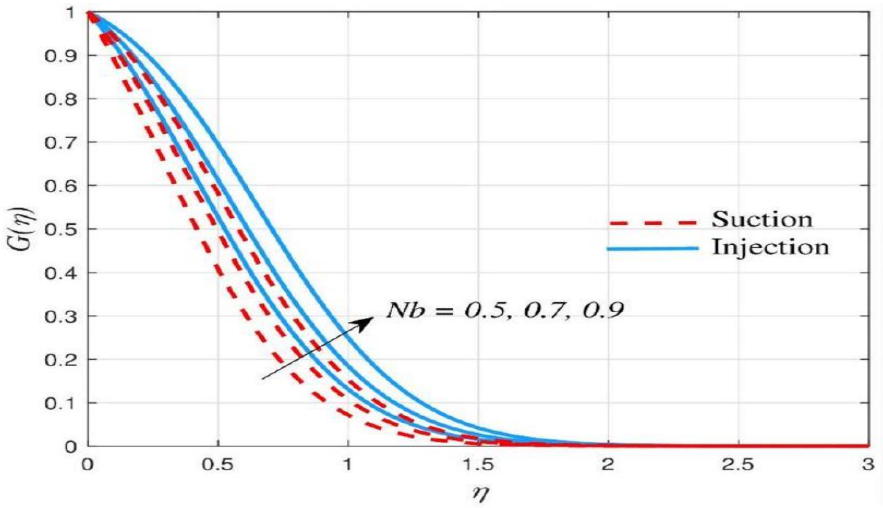


Fig. 4 Impact of $Nt$ over $G'(\eta)$ profile

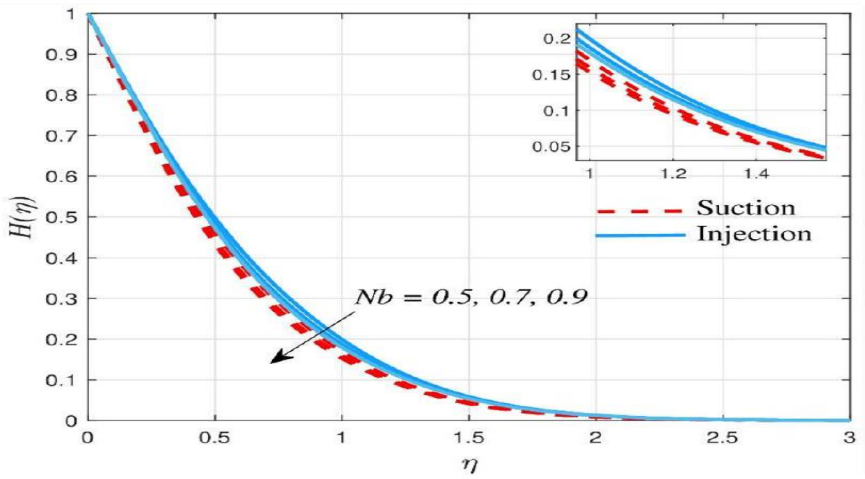


Fig. 5 Impact of $Nb$ over $H(\eta)$ profile

Figure 5: presents the influence of the Brownian motion parameter (Nb) on the concentration profile H′(η)H'(\eta)H′(η). As Nb increases, a decreasing trend in H′(η)H'(\eta)H′(η) is observed. Physically, higher Brownian motion enhances the random motion of nanoparticles, leading to a more uniform dispersion throughout the fluid. This effect lowers the concentration near the surface. The reduction in concentration is more noticeable in the suction case, where the fluid is drawn into the porous medium, reducing flow velocity and mass transfer rates. This lower pressure inhibits nanoparticle diffusion, resulting in a sharper decline in concentration compared to the injection scenario, where the fluid is forced into the domain, promoting dispersion.

Power System Technology
ISSN:1000-3673
Received: 16-04-2025 Revised: 05-05-2025 Accepted: 22-07-2025

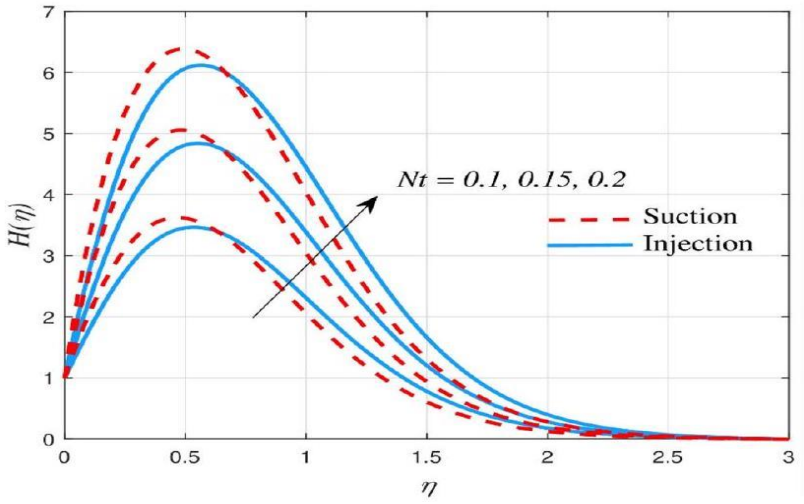


Fig. 6 Impact of $Nt$ over $H(\eta)$ profile

**Figure 6:** shows the effect of the thermophoresis parameter (Nt) on the concentration profile H′(η)H'(\eta)H′(η). An upward trend in concentration is seen with increasing Nt. This is due to thermophoresis forces driving nanoparticles away from the hot wall toward cooler fluid regions, leading to an accumulation of particles in certain areas and a net increase in concentration. This effect is more significant under injection conditions, where the flow drives concentrated fluid into the domain, further enhancing the concentration profile relative to the suction case.

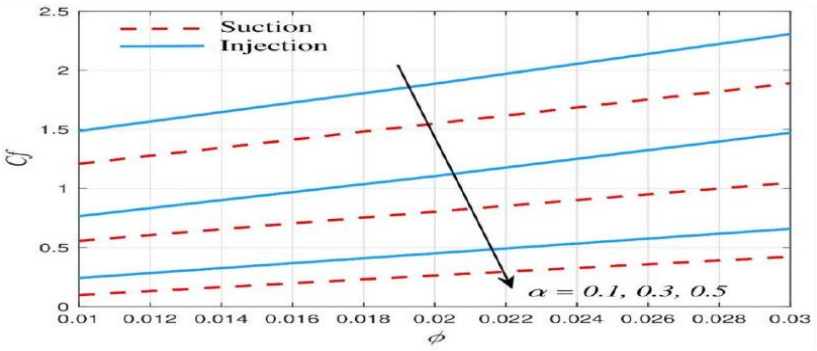


Fig. 7 Variations in $Cf$ for distinct values of $\alpha$

**Figure 7**: illustrates the impact of porosity (α) and nanoparticle volume fraction (ϕ) on the skin friction coefficient (Cf). Increased porosity corresponds to a more permeable medium, allowing smoother fluid passage through the porous matrix. This enhanced permeability reduces flow resistance and shear stress at the surface, thus decreasing skin friction. In suction scenarios, higher porosity facilitates easier fluid penetration, lowering drag. This

Power System Technology
ISSN:1000-3673
Received: 16-04-2025 Revised: 05-05-2025 Accepted: 22-07-2025

mechanism is beneficial in applications such as aircraft engineering, where suction through porous surfaces can suppress boundary layer separation, reduce drag, and significantly improve fuel efficiency.

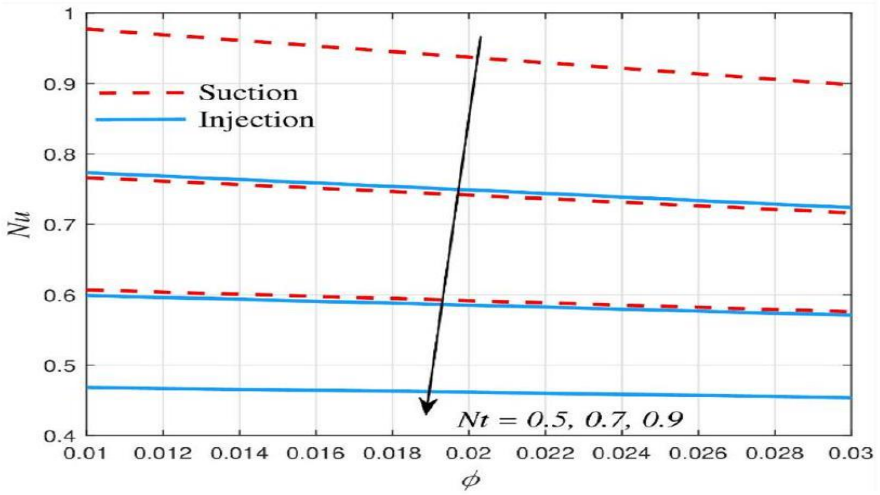


Fig. 8 Variations in $Nu$ for distinct values of $Nt$

**Figure 8:** depicts the variation in the Nusselt number (Nu) for increasing values of Nt and ϕ. A decreasing trend in Nu is observed with higher Nt values. Physically, as thermophoretic effects become more pronounced, particle migration increases, disrupting the thermal boundary layer and diminishing the convective heat transfer rate. This leads to a reduction in the Nusselt number, indicating weakened thermal transport performance.

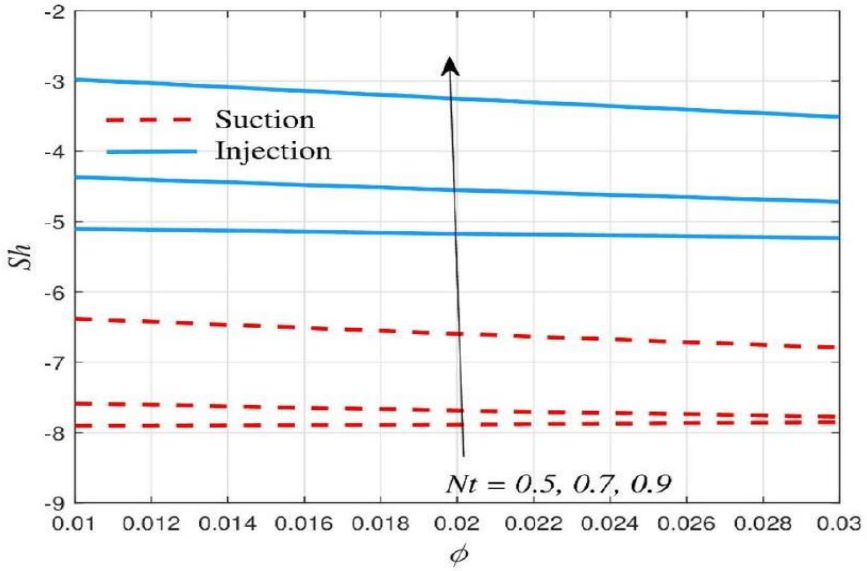


Fig. 9 Variations in (Sh) for distinct values of $Nt$

Power System Technology
ISSN:1000-3673
Received: 16-04-2025 Revised: 05-05-2025 Accepted: 22-07-2025

**Figure 9:** illustrates the variations in the Sherwood number (Sh) for different values of the thermophoresis parameter (Nt), which contribute to an increase in the temperature profile. This rise in temperature is more pronounced in the injection case compared to suction. Under suction conditions, cooler ambient fluid is drawn towards the surface, reducing the thickness of the thermal boundary layer and limiting the temperature increase. In contrast, during injection, the heated fluid moves away from the surface, thickening the thermal boundary layer and allowing a more significant rise in temperature.As a result, the Nusselt number (Nu) exhibits a decreasing trend with increasing Thermophoresis parameter (Nt). In the injection case, this effect is more pronounced due to the thickening of the thermal boundary layer, which enables greater accumulation of nanoparticles near the wall. This accumulation disrupts heat transfer, causing a sharper decline in Nu compared to the suction case. In practical applications, particularly electronic cooling systems such as CPUs and power modules, optimizing coolant injection while accounting for thermophoretic behavior can significantly enhance thermal management efficiency.further illustrates the impact of Nt and $\phi$ on the Sherwood number (Sh). As Nt increases, a corresponding rise in Sh is observed, indicating improved mass transfer. Physically, a stronger thermophoretic force induced by higher temperature gradients promotes a more uniform dispersion of nanoparticles, which enhances convective mass transport. This effect is amplified under injection conditions, where increased fluid motion strengthens mass transfer mechanisms, resulting in a higher Sherwood number. In systems like electronics or HVAC cooling units, a higher Sh implies more efficient transport of mass (e.g., heat or species) from surfaces to the working fluid, thus enhancing cooling performance and lowering energy consumption.

**Table 4**

| β | S | α | ϕ | Le | Nt | Nb | Cf | Nu | Sh |
|---|---|---|---|---|---|---|---|---|---|
| 0.5 | 0.5 | 1.5 | 0.01 | 0.8 | 0.3 | 0.3 | -0.76549 | 1.57045 | -0.40868 |
| 1.0 | 0.5 | 1.5 | 0.01 | 0.8 | 0.3 | 0.3 | -0.40800 | 1.56542 | -0.42281 |
| 1.5 | 0.5 | 1.5 | 0.01 | 0.8 | 0.3 | 0.3 | -0.28506 | 1.56081 | -0.43096 |
| 0.5 | -0.5 | 1.5 | 0.01 | 0.8 | 0.3 | 0.3 | -0.49500 | 1.30500 | -0.22500 |
| 0.5 | 0.0 | 1.5 | 0.01 | 0.8 | 0.3 | 0.3 | -0.44557 | 1.42768 | -0.31728 |
| 0.5 | 0.5 | 1.5 | 0.01 | 0.8 | 0.3 | 0.3 | -0.40800 | 1.56542 | -0.42281 |
| 0.5 | 0.5 | 1.5 | 0.01 | 0.8 | 0.3 | 0.3 | -0.22211 | 1.52554 | -0.43324 |
| 0.5 | 0.5 | 1.5 | 0.01 | 0.8 | 0.4 | 0.3 | -0.20780 | 1.51880 | -0.44000 |
| 0.5 | 0.5 | 1.5 | 0.01 | 0.8 | 0.3 | 0.3 | -0.18934 | 1.51235 | -0.43555 |
| 0.5 | 0.5 | 1.5 | 0.01 | 0.8 | 0.3 | 0.3 | -0.38676 | 1.66537 | -0.45576 |
| 0.5 | 0.5 | 1.5 | 0.02 | 0.8 | 0.3 | 0.3 | -0.39424 | 1.61472 | -0.43920 |

Power System Technology
ISSN:1000-3673
Received: 16-04-2025 Revised: 05-05-2025 Accepted: 22-07-2025

| β | S | α | ϕ | Le | Nt | Nb | Cf | Nu | Sh |
|---|---|---|---|---|---|---|---|---|---|
| 0.5 | 0.5 | 1.5 | 0.03 | 0.8 | 0.3 | 0.3 | -0.40800 | 1.56542 | -0.42281 |
| 0.5 | 0.5 | 1.5 | 0.01 | 0.8 | 0.3 | 0.3 | -0.40800 | 1.56542 | -0.42281 |
| 0.5 | 0.5 | 1.5 | 0.01 | 1.0 | 0.3 | 0.3 | -0.40500 | 1.57218 | -0.59178 |
| 0.5 | 0.5 | 1.5 | 0.01 | 1.2 | 0.3 | 0.3 | -0.38434 | 1.57819 | -0.75447 |
| 0.5 | 0.5 | 1.5 | 0.01 | 0.8 | 0.5 | 0.3 | -0.40978 | 1.54664 | -0.76006 |
| 0.5 | 0.5 | 1.5 | 0.01 | 0.8 | 0.7 | 0.3 | -0.40197 | 1.52809 | -1.08687 |
| 0.5 | 0.5 | 1.5 | 0.01 | 0.8 | 0.3 | 0.5 | -0.40800 | 1.56542 | -0.18000 |
| 0.5 | 0.5 | 1.5 | 0.01 | 0.8 | 0.3 | 0.7 | -0.40195 | 1.54738 | -0.14204 |
| 0.5 | 0.5 | 1.5 | 0.01 | 0.8 | 0.3 | 0.3 | -0.40195 | 1.52944 | 0.05000 |

**Table 4:** summarizes the influence of various key parameters—such as porosity α, Brownian motion Nb, and Thermophoresis Nt—on the engineering characteristics: skin friction coefficient (Cf), Nusselt number (Nu), and Sherwood number (Sh). These trends highlight the critical role of nanoparticle dynamics and flow control strategies (like suction and injection) in optimizing thermal and mass transport in hybrid nanofluid applications.

**References**

1. Hussain, Z., Ayaz, M., & Islam, S. (2024). Effects of thermophoresis and Brownian motion on radiative MHD hybrid nanofluid flow over a stretching sheet with convective boundary conditions: A homotopic approach. *Multidiscipline Modeling in Materials and Structures*. https://doi.org/10.1177/23977914231225019SAGE Journals
2. Alreshidi, N. A., Shah, Z., Dawar, A., Kumam, P., Shutaywi, M., &Watthayu, W. (2020). Brownian motion and thermophoresis effects on MHD three-dimensional nanofluid flow with slip conditions and Joule dissipation due to porous rotating disk. *Molecules*, 25(3), 729. https://doi.org/10.3390/molecules25030729MDPI
3. Wang, R., Du, J., & Zhu, Z. (2016). Effects of wall slip and nanoparticles' thermophoresis on the convective heat transfer enhancement of nanofluid in a microchannel. *Journal of Thermal Science and Technology*, 11(1), JTST00017. https://doi.org/10.1299/jtst.2016jtst00017J-STAGE
4. Raju, C. S., JayachandraBabu, M., & Sandeep, N. (2016). Chemically reacting radiative MHD Jeffrey nanofluid flow over a cone in porous medium. *International Journal of Engineering Research in Africa*, 19, 75–90. https://doi.org/10.4028/www.scientific.net/JERA.19.75MDPI
5. Kumar, A., Ray, R. K. (2022). Shape effect of nanoparticles and entropy generation analysis for magnetohydrodynamic flow of ($Al_2O_3$–Cu/$H_2O$) hybrid nanomaterial under

Power System Technology
ISSN:1000-3673
Received: 16-04-2025 Revised: 05-05-2025 Accepted: 22-07-2025

the influence of Hall current. *Indian Journal of Physics*, 96(13), 3817–3830. https://doi.org/10.1007/s12648-022-02300-8

6. Zaidi, S. Z. A., Mohyud-din, S. T., & Bin-Mohsen, B. (2017). A comparative study of wall jet flow containing carbon nanotubes with convective heat transfer and MHD. *Engineering Computations*, 34(3), 739–753. https://doi.org/10.1108/EC-03-2016-0087
7. Jafarimoghaddam, A., &Shafizadeh, F. (2019). Numerical modeling and spatial stability analysis of the wall jet flow of nanofluids with thermophoresis and Brownian effects. *Propulsion and Power Research*, 8(3), 210–220. https://doi.org/10.1016/j.jppr.2019.06.002
8. Khan, U., Zaib, A., &Ishak, A. (2023). Impact of thermal and activation energies on Glauert wall jet heat and mass transfer flows induced by ZnO–SAE50 nano lubricants with chemical reaction: The case of Brinkman-Extended Darcy model. *Lubricants*, 11(1), 22. https://doi.org/10.3390/lubricants11010022
9. Ganga, S., Uddin, Z., & Asthana, R. (2023). Modelling of viscosity and thermal conductivity of water-based nanofluids using machine-learning techniques. *International Journal of Mathematical, Engineering and Management Sciences*, 8(5), 817–840. https://doi.org/10.33889/IJMEMS.2023.8.5.047
10. Alzahrani, H. A. H., Alsaiari, A., Madhukesh, J. K., Kumar, R. N., &Prasanna, B. M. (2022). Effect of thermal radiation on heat transfer in plane wall jet flow of Cassonnanofluid with suction subject to a slip boundary condition. *Waves in Random and Complex Media*, 1–18. https://doi.org/10.1080/17455030.2022.2030502
11. Ali Zaidi SZ, Mohyud-din ST, Bin-Mohsen B (2017) A comparative study of wall jet flow containing carbon nanotubes with convective heat transfer and MHD. Eng Comput 34(3):739–753.https://doi.org/10.1108/EC-03-2016-0087
12. Aly EH, Mahabaleshwar US, Anusha T, Usafzai WK, Pop I (2022) Wall jet flow and heat transfer of a hybrid nanofluid subject to suction/injection with thermal radiation. ThermSciEngProg 32:101294. https://doi.org/10.1016/j.tsep.2022.101294
13. Aly EH, Khan Usafzai W, Merkin JH, Pop IM (2024) Viscous fluid flow and heat transfer past a permeable wall jet with convective boundary conditions. Multidiscip Model Mater Struct 20(4):658–670. https://doi.org/10.1108/MMMS-11-2023-0362
14. Alzahrani HAH et al (2022) Effect of thermal radiation on heat transfer in plane wall jet flow of Cassonnanofluid with suction subject to a slip boundary condition. Waves Random Complex Media.https:// doi.org/10.1080/17455030.2022.2030502
15. Babu TL, Gannamaraju KK, Rajashekar MN (2024) Joint effects of Brownian motion and thermophoresis on Williams on nano fluid flow past a stretching sheet: MHD and chemical reaction effects. J Adv Res Fluid Mech Therm Sci 120(1):68–84.https://doi.org/10. 37934/arfmts.120.1.6884

Power System Technology
ISSN:1000-3673
Received: 16-04-2025 Revised: 05-05-2025 Accepted: 22-07-2025

16. Chaurasiya VK, Kumar A, Tripathi R, Singh R (2024) Impact of magnetic induction on the flow of self-rewetting power-law fluid over a disk surface: onset of Marangoni convection". Heat Transf. Part Appl, Numer. https://doi.org/10.1080/10407782.2024.2343041
17. GangaS,UddinZ,AsthanaR,HassanH,BhardwajA(2023)Modelling of viscosity and thermal conductivity of water-based nanofluids using machine-learning techniques. Int J Math EngManagSci 8(5):817–840. https://doi.org/10.33889/IJMEMS.2023.8.5.047
18. Ganga S, Uddin Z, Asthana R (2025) Exploring swirling flow dynamics: unsupervised machine learning in Maxwell hybrid nanofluid convection over an exponentially stretching cylinder with nonlinear radiation effects. Commun Nonlinear SciNumer Simul 140:108378. https://doi.org/10.1016/j.cnsns.2024.108378
19. Jafarimoghaddam A, Shafizadeh F (2019) Numerical modeling and spatial stability analysis of the wall jet flow of nanofluids with thermophoresis and Brownian effects. Propuls Power Res 8(3):210–220. https://doi.org/10.1016/j.jppr.2019.06.002
20. Khan U et al (2023a) Analysis of assisting and opposing flows of the Eyring-Powell fluid on the wall jet nanoparticles with significant impacts of irregular heat source/sink. Case Stud ThermEng 49:103209. https://doi.org/10.1016/j.csite.2023.103209
21. Khan U, Zaib A, Ishak A (2023b) Impact of thermal and activation energies on Glauert Wall Jet (WJ) heat and mass transfer flows induced by ZnO-SAE50 nano lubricants with chemical reaction: thecaseofBrinkman-ExtendedDarcymodel.Lubricants11(1):22. https://doi.org/10.3390/lubricants11010022
22. Khan Usafzai W, Haq RU, Aly EH (2023) Wall laminar nanofluid jet flow and heat transfer. Int J Numer Methods Heat Fluid Flow 33(5):1818–1836. https://doi.org/10.1108/HFF-09-2022-0528
23. Köten H, Shaikh GM, Memon AA, Memon MA, Yashkun U, Obalalu AM (2024) Numerical study of flow behavior and heat transfer of ternary water- based nanofluids in the presence of suction/injection, stretching/shrinking sheet. J ThermEng 10(4):1021–1043
24. Kumar A, Ray RK (2022) Shape effect of nanoparticles and entropy generation analysis for magnetohydrodynamic flow of ($Al_2O_3 - Cu/H_2O$)hybrid nanomaterial under the influence of Hall current. Indian J Phys 96(13):3817–3830.https://doi.org/10.1007/s12648-022-02300-8
25. Kumar A, Singh R, Seth GS, Tripathi R (2018a) Double diffusive magnetohydrodynamic natural convection flow of Brinkman type nanofluid with diffusion-thermo and chemical reaction effects. J Nanofluids 7(2):338–349. https://doi.org/10.1166/jon.2018.1455 KumarA,SinghR,ShankerSG,TripathiR(2018b) Soreteffectontransientmagnetohydrodynamicnanofluid flow past a vertical plate through a porous